Supplement of Clim. Past, 18, 713–738, 2022
https://doi.org/10.5194/cp-18-713-2022-supplement

Climate of the Past
Open Access
EGU

Supplement of

Secular and orbital-scale variability of equatorial Indian Ocean summer monsoon winds during the late Miocene

Clara T. Bolton et al.

Correspondence to: Clara T. Bolton (bolton@cerege.fr)

Table S1: Splice table for Site U1443 late Miocene interval.

Site	Hole	Core	Type	Top section	Top offset (cm)	Top depth CSF-A (m)	Top depth CCSF-A (m)	Bottom section	Bottom offset (cm)	Bottom depth CSF-A (m)	Bottom depth CCSF-A (m)	Comments
U1443	C	9	H	2	46	63.06	70.40	6	81	69.41	76.74	Revised shipboard 2015
U1443	B	8	H	2	149	68.99	76.74	5	131	73.31	81.06	Revised shipboard 2015
U1443	C	10	H	2	83	72.93	81.06	7	55	79.05	87.18	Revised shipboard 2015
U1443	B	9	H	3	2	78.29	87.18	4	129	81.06	89.96	Revised shipboard 2015
U1443	C	11	H	1	38	80.48	89.96	3	28	83.38	92.86	Revised shipboard 2015
U1443	A	10	H	1	67	78.47	92.86	6	57	85.87	100.26	Revised shipboard 2015
U1443	C	12	H	2	63	91.73	100.26	3	135	93.95	102.49	Revised shipboard 2015
U1443	B	11	H	1	125	92.75	102.49	6	55	99.11	108.85	Revised shipboard 2015
U1443	A	11	H	5	61	93.84	108.85	7	19	96.22	111.23	Revised shipboard 2015
U1443	C	13	H	4	65	102.25	111.23	5	78	103.88	112.86	Revised shipboard 2015
U1443	B	12	H	1	101	102.01	112.87	6	50	109	119.86	Revised Lübbers 2019
U1443	C	15	H	3	9	108.69	119.86	5	32	111.92	123.1	Revised Lübbers 2019
U1443	B	13	H	1	63	111.13	123.10	5	86	117.01	128.99	Revised Lübbers 2019
U1443	C	16	H	2	101	117.61	128.99	6	9	122.69	134.08	Revised Lübbers 2019
U1443	B	14	H	1	82	120.82	134.08	5	139	127.39	14.66	Revised Lübbers 2019

Table S2: Site U1443 late Miocene revised nannofossil biostratigraphy

Event (nannofossil)	Age, Ma (Gradstein et al., 2012)	Top CCSF (m)	Bottom CCSF (m)	Mid-depth CCSF (m)	Error (m) (±)
T Ceratolithus acutus	5.04	70.06	71.04	70.55	0.49
T Triquetrorhabdulus rugosus	5.28	too rare to reliably define			
B Ceratolithus acutus	5.35	76.22	77.06	76.64	0.42
T Discoaster quinqueramus	5.59	78.10	78.53	78.31	0.22
B N. amplificus	6.91	95.15	96.13	95.64	0.49
B D. quinqueramus	8.12	111.70	112.69	112.19	0.50
B D. berggreni	8.29	112.69	113.40	113.04	0.36
T Discoaster hamatus	9.53	125.50	125.90	125.70	0.20

T= top (last occurrence)

B=base (first occurrence)

Table S3: Site U1443 ET tuning tie-points

U1443 depth (m CCSF)	Age (Ma)	Sedimentation rate (cm/kyr)
70.72	4.997	1.76
74.22	5.195	1.05
75.55	5.322	1.27
77.10	5.444	1.25
78.60	5.564	1.20
81.15	5.777	1.40
84.50	6.017	1.23
85.52	6.100	1.67
88.92	6.304	1.27
90.99	6.468	1.02
93.10	6.674	1.36
95.38	6.843	1.16
96.73	6.960	1.50
98.54	7.080	1.34
100.71	7.243	1.06
101.99	7.363	1.05
102.82	7.442	1.71
104.90	7.564	1.52
106.74	7.685	1.25
108.87	7.855	1.87
111.78	8.011	1.23
113.36	8.140	1.58
115.85	8.297	1.41
118.74	8.502	1.41
119.86	8.581	1.07
120.72	8.662	0.64
121.28	8.750	0.53
121.91	8.868	0.72
122.53	8.953	

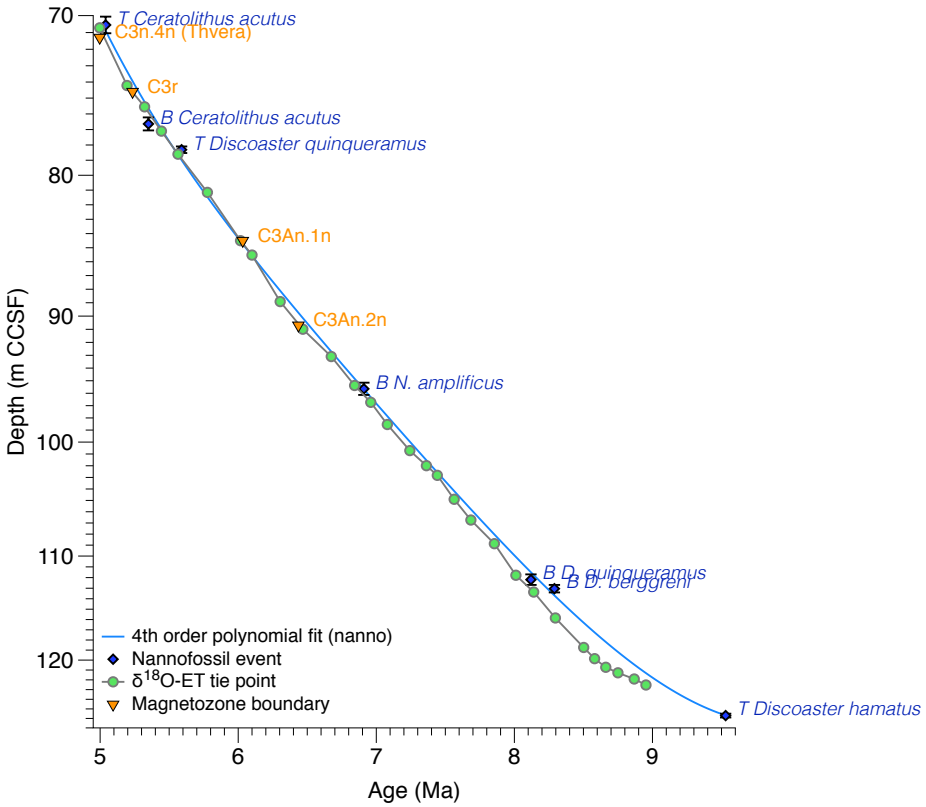

Figure S1: Age-depth plot for Site U1443. Revised nannofossil events are shown with errors in the depth domain, and a 4th order polynomial fit. Magnetozone boundaries are from Clemens et al. (2016). Ages follow Gradstein et al. (2012). Tie-points for the orbitally-tuned age model are shown in green, and we assume linear sedimentation rates between tie points.

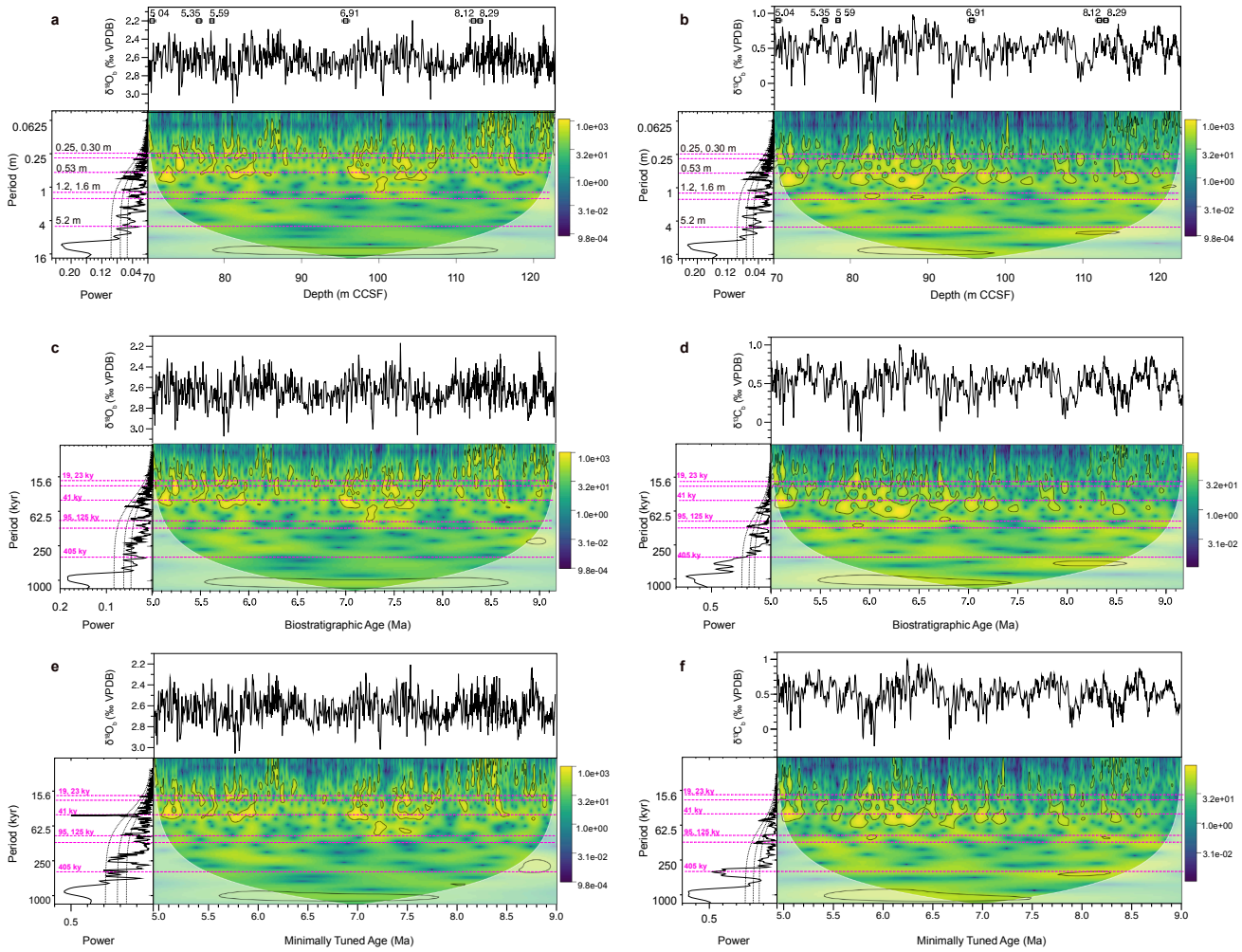

Figure S2: Spectral analyses of Site U1443 bandpassed benthic $\delta^{18}O$ and $\delta^{13}C$ records in the depth domain (**a**, **b**), on the revised biostratigraphic age model (4th polynomial fit, Fig. S1) (**c**, **d**), and on the final orbitally-tuned age model (**e**, **f**). Contour lines in wavelet plots denote 95% significance. Lines in MTM spectral analyses (left panels) show 90%, 95%, and 99% confidence levels using a robust red nose model. Main primary orbital periods are shown as pink lines. In **a** and **b**, depth periods shown correspond to the same orbital periods shown in other panels assuming a constant sedimentation rate of 1.29 cm/kyr, which corresponds to the average based on the biostratigraphic age model.

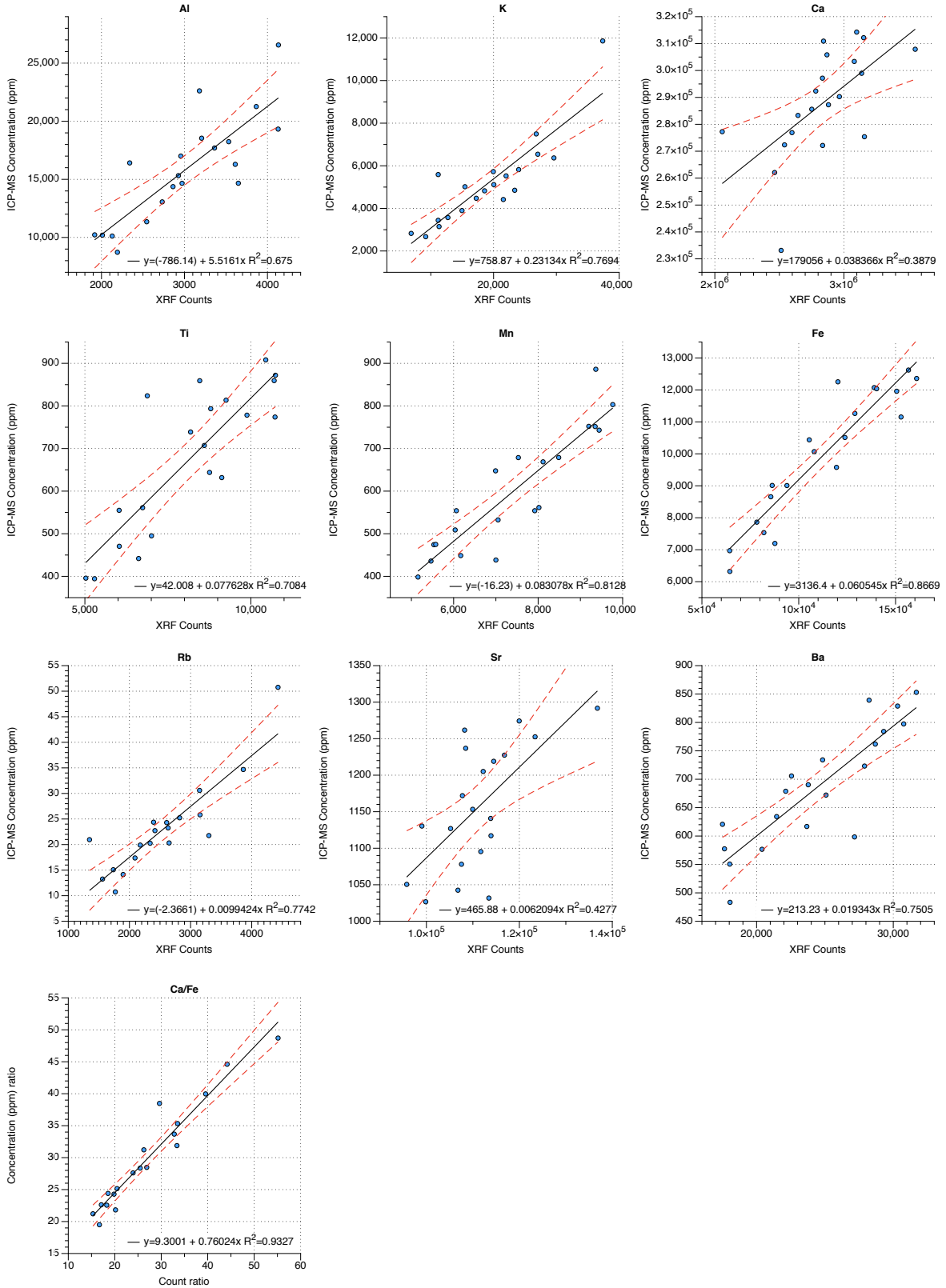

Figure S3: XRF calibration results based on linear relationships between raw counts and elemental concentrations. Red lines show 95% confidence bounds around linear fits.

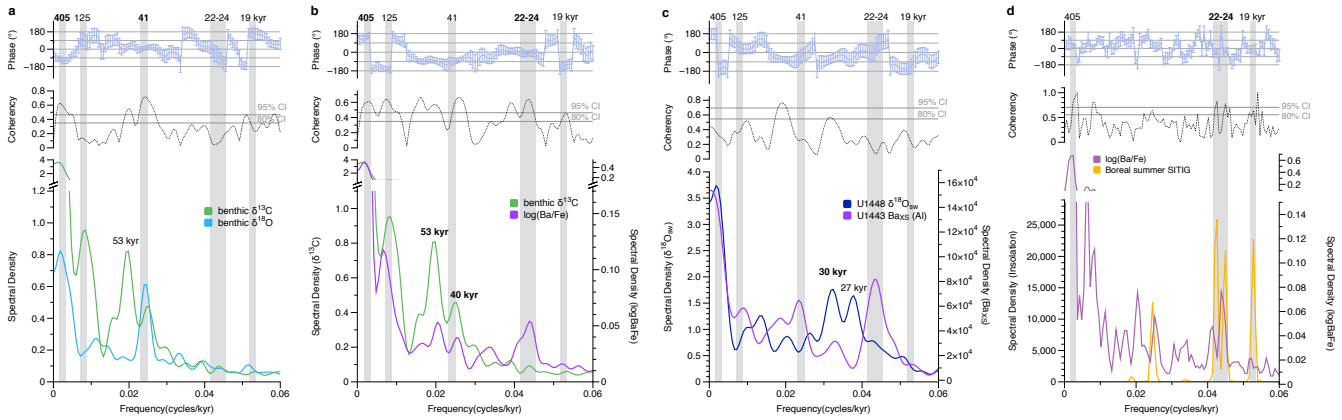

Figure S4: Cross-spectral analyses between (a) benthic $\delta^{18}O$ and $\delta^{13}C$ (9-5 Ma), and (b) benthic $\delta^{13}C$ and log(Ba/Fe) (9-5 Ma), (c) Ba_{xs} at Site U1443 and $\delta^{18}O_{sw}$ at Site U1448 (Jöhnck et al., 2020) (6.2-5 Ma), (d) The summer inter-tropical insolation gradient (SITIG) (Laskar et al., 2004) and log(Ba/Fe) (9-5 Ma).

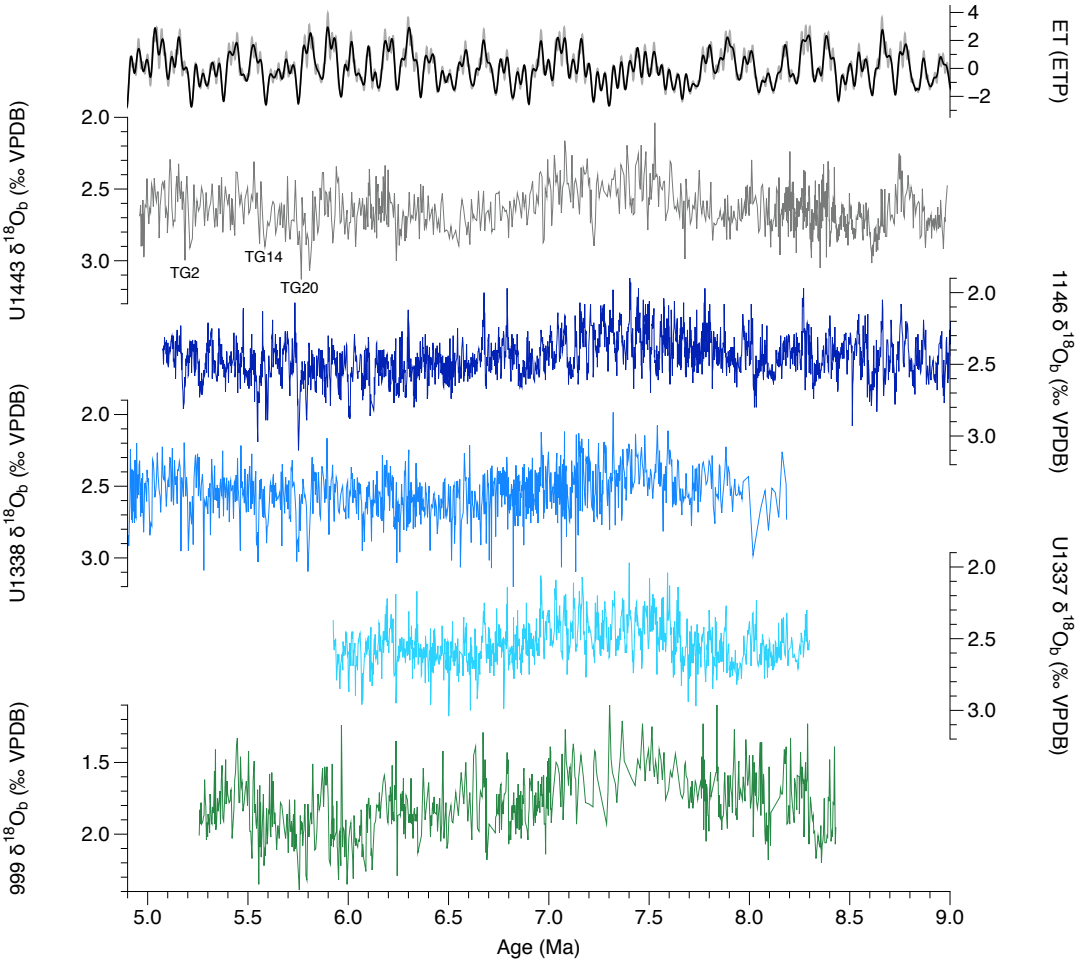

Figure S5: Comparison of the Site U1443 Indian Ocean $\delta^{18}O$ record (*C. wuellerstorfi*) with coeval high-resolution records from Pacific (blue colours) and Atlantic (green colours) low-latitude sites: South China Sea ODP 1146 (*C. wuellersorfi* and *C. mundulus*) (Holbourn et al., 2018; Holbourn et al., In Press), equatorial Pacific IODP Sites U1338 (*C. mundulus*) (Drury et al., 2018; Drury et al.,

2016) and U1337 (*C. mundulus*) (Drury et al., 2017), and Caribbean ODP Site 999 (*C. wuellerstorfi*) (Bickert et al., 2004). All records are shown on their latest independent orbitally-tuned chronologies, except for Site 999, where the age model was constructed via correlation to ODP Sites 982 and 926 (Bickert et al., 2004). All values are raw (uncorrected).

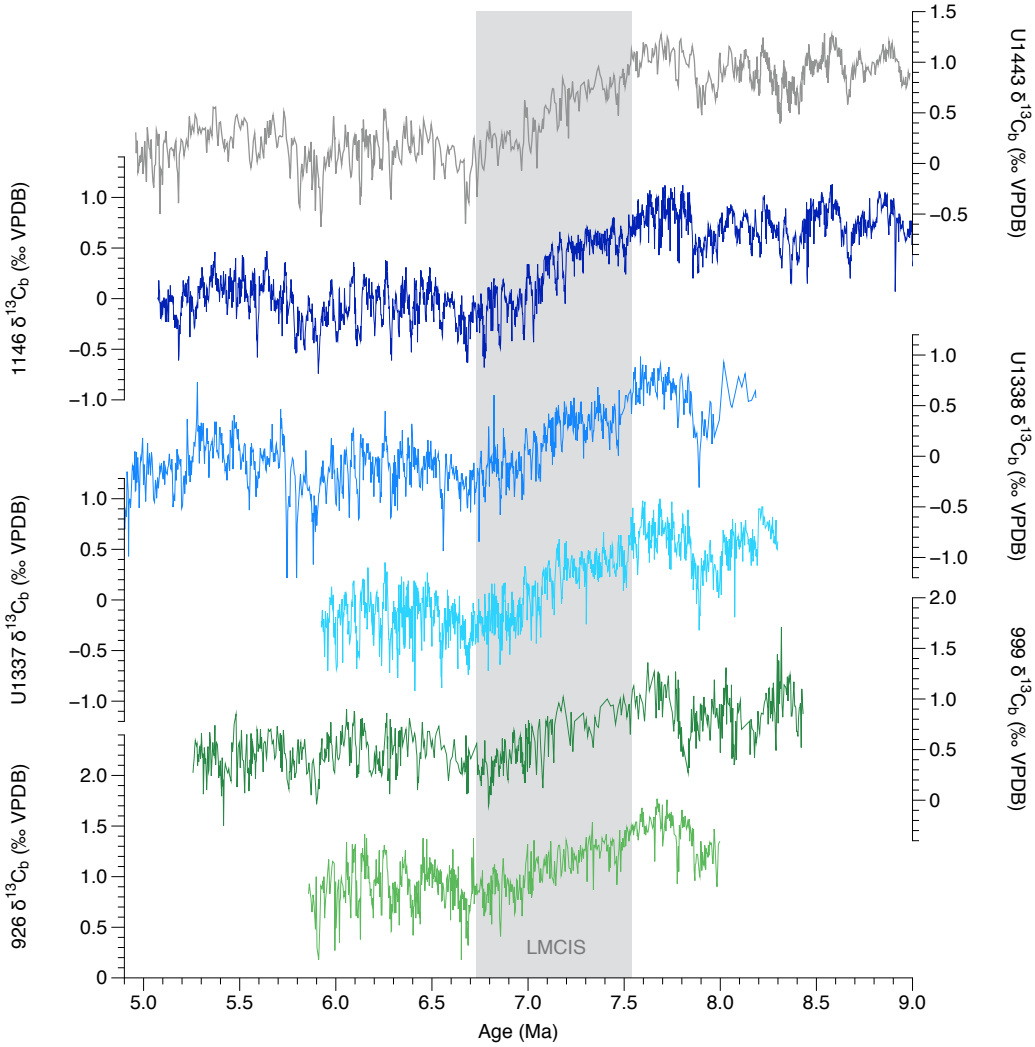

Figure S6: Comparison of the Site U1443 Indian Ocean $\delta^{13}C$ record with coeval high-resolution records from Pacific (blue colours) and Atlantic (green colours) low-latitude sites. Sites and references as in Figure 4, with the addition of ODP Site 926 (mixed species) (Shackleton and Hall, 1997; Drury et al., 2017; Zeeden et al., 2013). All $\delta^{13}C$ values are raw, except the ODP Site 926 record that includes corrections for some samples due to its multispecific nature, using offsets cited in the original publication (Drury et al., 2017). LMCIS = Late Miocene carbon isotope shift, with its duration following (Drury et al., 2017).

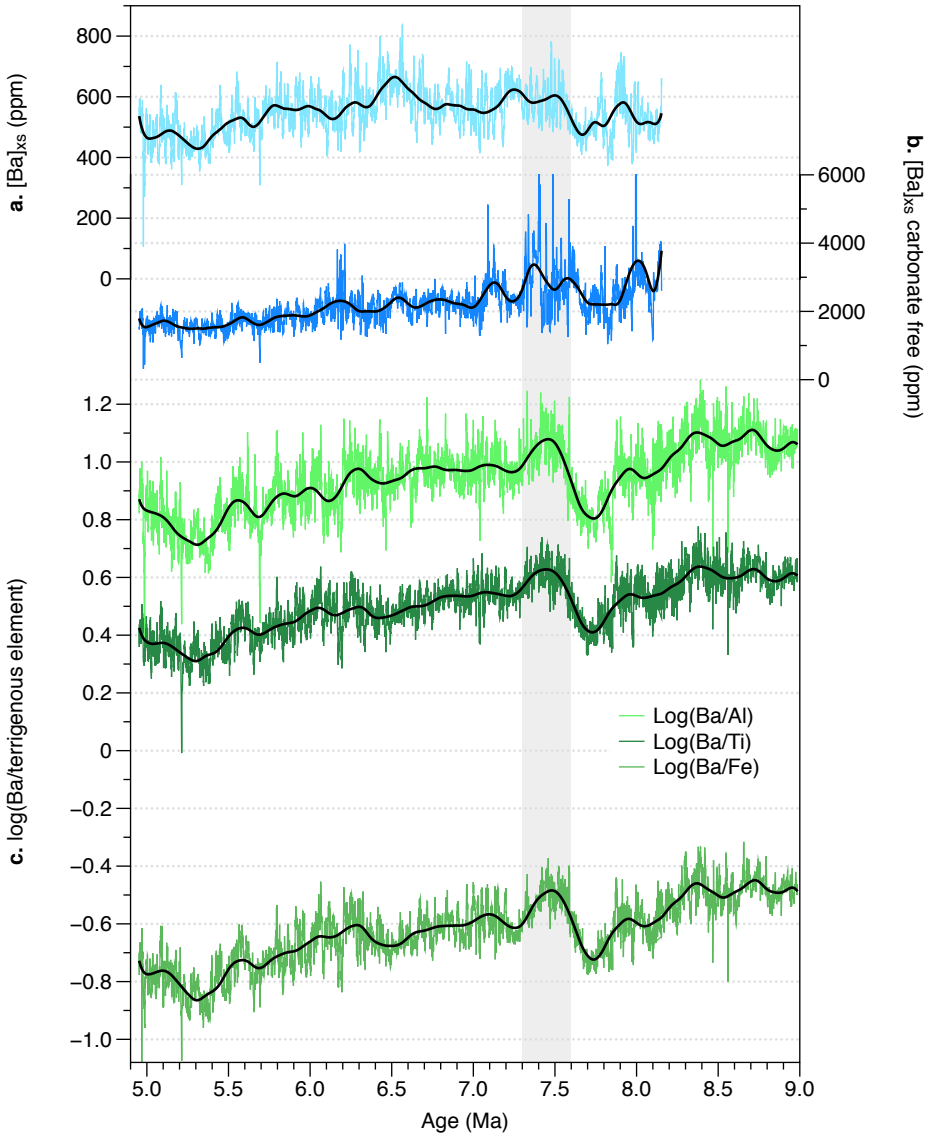

Figure S7: Comparison of biogenic barium records. **a**: $[Ba]_{xs}$, **b**: carbonate-free $[Ba]_{xs}$, **c**: comparison of log(Ba/Al), log(Ba/Fe) and log (Ba/Ti).